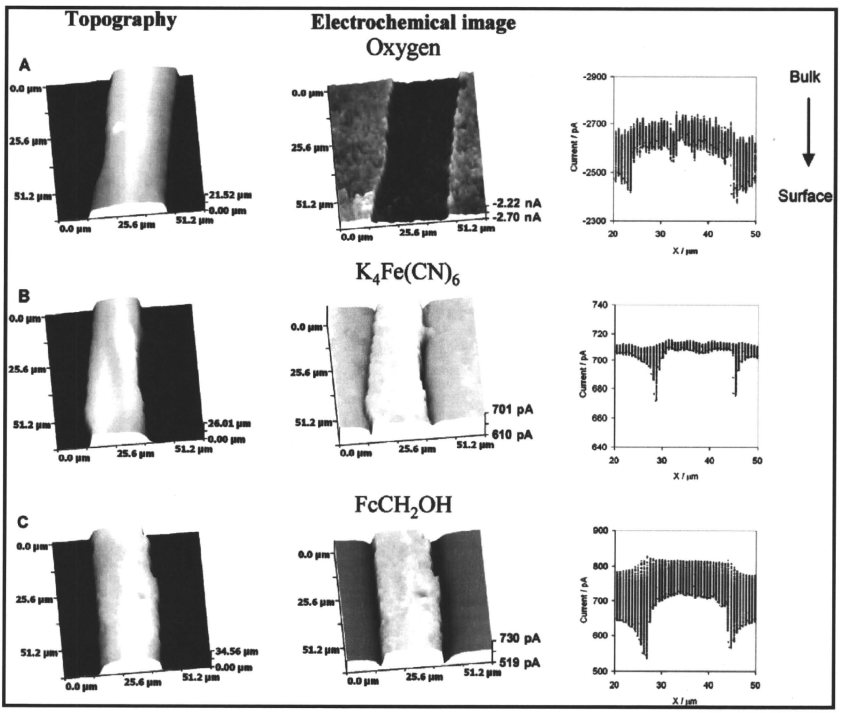

Figure 9. Topographic (left) and electrochemical (center) images of a rat cardiac myocyte and electrochemical signal profiles of repeated approach curves at each measurement point (right). Electrochemical images were based on (A) reduction current of oxygen at −500 mV vs Ag/AgCl, (B) oxidation current of 0.50 mM $K_4Fe(CN)_6$ at 500 mV vs Ag/AgCl, and (C) oxidation current of 0.50 mM $FcCH_2OH$ at 500 mV vs Ag/AgCl. The SICM nanopipette electrode was held at 200 mV vs Ag/AgCl. Scan ranges were 64 μm × 64 μm. The approach distances were set to 10 μm. Arrows and dashed lines denote the direction of the approach and boundaries of the cell and substrate, respectively.

$FcCH_2OH$ associated with the cellular inner enzyme activity was detected. This is the first time that simultaneous characterization of the localized permeation property of a living cell membrane and cellular surface topography imaging was achieved. In our experiment, strict estimation of membrane permeability is difficult because the complicated shape of the electrode used. However, it is possible to compare the membrane permeation property, by using same electrode under the same experimental conditions.

Conclusion

We developed a SECM/SICM system with a hybrid nanoprobe consisting of a nanoring electrode for electrochemical measurements and a nanopipette for ion current measurement as a feedback signal. This system enables simultaneous submicrometer scale electrochemical and noncontact topography measurements. Furthermore, we adopted the hopping scanning mode for ion current distance regulation to achieve convoluted living cellular surface topography measurements and detection of the spatial distribution of electrochemical species. The present system will be applicable to detailed analysis of membrane surface phenomena that are induced by a nanopipette providing specific biomolecules locally.

Acknowledgment. This work was partly supported by a Grant-in-Aid for Scientific Research (18101006) from MEXT (Ministry of Education, Culture, Sports, Science and Technology), Japan. Y.T. acknowledges the support obtained from a research fellowship of the Japan Society for the Promotion of Science.

Supporting Information Available: The evaluation of the interference of the SECM nanoring electrode and SICM nanopipette electrode. SECM/SICM topography image comparison with AFM image. This material is available free of charge via the Internet at http://pubs.acs.org.

JA1029478

FEBS Letters 584 (2010) 4000–4008

ELSEVIER

FEBS Letters

journal homepage: www.FEBSLetters.org

Reporter gene expression at single-cell level characterized with real-time RT-PCR, chemiluminescence, fluorescence, and electrochemical imaging

Hitoshi Shiku [a,*], Daisuke Okazaki [a], Junya Suzuki [a], Yasufumi Takahashi [a], Tatsuya Murata [a], Hidetaka Akita [b], Hideyoshi Harashima [b], Kosuke Ino [a], Tomokazu Matsue [a,**]

[a] Graduate School of Environmental Studies, Tohoku University, Aramaki-Aoba 6-6-11, Sendai 980-8579, Japan
[b] Faculty of Pharmaceutical Sciences, Hokkaido University, Kita 12 Nishi 6, Kita-Ku, Sapporo, Hokkaido 060-0812, Japan

ARTICLE INFO

Article history:
Received 24 May 2010
Revised 31 July 2010
Accepted 5 August 2010
Available online 11 August 2010

Edited by Paul Bertone

Keywords:
Transcription
Translation
Single-cell analysis
Reporter assay

ABSTRACT

mRNA from single cells was quantified using real-time RT-PCR after recording the address and reporter protein activity with chemiluminescence, fluorescence, and electrochemical techniques, using luciferase, green fluorescent protein, and secreted alkaline phosphatase. mRNA copy number ranging from below 10^3 to 10^7 in single cells showed a lognormal distribution for both externally introduced reporter genes and internally expressed genes. The fluctuation in the gene expression decreased with the increase of the number of cells picked but did not decrease with the increase of mRNA copy number per cell. We found that the correlation coefficients for mRNA and protein expression in logarithmic plot at single-cell level were much lower than 1.00.

1. Introduction

Single-cell analysis has become important in the attempt to understand the mechanisms underlying the principles of life science, especially the fundamental nature of diversity and plasticity in biological cellular systems. Typical examples illustrating the significance of single-cell analysis are provided by surveys of multipotent marker proteins in various stem cell systems and differentiation processes [1–3]. It is now recognized that the level of gene expression varies widely at the single-cell level in undifferentiated cells, even for cells from clonal populations. Surprisingly, sorted cellular fractions with higher or lower expression levels of a stem cell marker started to change their distribution within 9 h of culture, but reestablished the original broad distribution after 216 h [1]. Another field of study is single-cell noise analysis in which reporter genes were introduced into bacteria [4,5], yeast [6], or mammalian cells [7,8]. Mathematical models were introduced for the quantitative analysis of the dynamics and stability of cellular status at the genome, transcriptome, proteome, and/or metabolome levels. This type of single-cell study showed that the mRNA [9–17] and protein expression [1–8] levels show extreme fluctuation in not only undifferentiated but also all kinds of cells.

However, experimental system to simultaneously monitor the expression levels of mRNAs and proteins in a single-cell experimental system has been limited in the present stage. Raj et al. investigated the correlation between protein and mRNA expressions of GFP from fixed individual mammalian cells [7]. In their experiment, the protein and mRNA were quantified by fluorescence imaging and fluorescence in situ hybridization (FISH), respectively. However, FISH it not appropriate to quantify more than 10^3 copies of mRNA molecules. In contrast, PCR-based mRNA analysis is expected to provide information about single-cell gene expression with a much wider dynamic range. Single-cell PCR analysis has been successfully applied to analyze stochastic nature of single-cell system based on lognormal distribution of mRNA copy number per cell by utilizing manual cell picking [9], microfluidic digital PCR device [10], and laser microdissection [17]. Unfortunately, these techniques have not been applied yet for mRNA analysis with extremely large mRNA copy number per cell.

In the present study, mRNAs and proteins from individual cells were quantified in three reporter systems: luciferase (Luc), green fluorescent protein (GFP), and secreted alkaline phosphatase (SEAP). The three types of reporter protein were evaluated using chemiluminescence (CL), fluorescence (FL), and electrochemical techniques, respectively. For each cell, we quantified the protein expression level and estimated the mRNA expression level by

* Corresponding author. Fax: +81 22 795 7209.
** Corresponding author.
E-mail addresses: shiku@bioinfo.che.tohoku.ac.jp (H. Shiku), matsue@bioinfo.che.tohoku.ac.jp (T. Matsue).

0014-5793/$36.00 © 2010 Federation of European Biochemical Societies. Published by Elsevier B.V. All rights reserved.
doi:10.1016/j.febslet.2010.08.008

real-time RT-PCR (RT-qPCR). HeLa cells transfected with several plasmid vectors were used as a model single-cell system to verify whether stochastic nature was still observed or not for an extremely higher mRNA expression activity with 10^7 copies per cell.

2. Materials and methods

2.1. Chemicals and materials

RPMI-1640 (Gibco Invitrogen, Tokyo, Japan), fetal bovine serum (FBS; Gibco), penicillin/streptomycin (Gibco), Opti-MEM I medium (Gibco), Lipofectamine™ 2000 (Invitrogen), 3,3,4,4,5,5,6,6,6-non-afluorohexyl trichlorosilane (LS-912; Shin-Etsu Chemical Co. Ltd.), and other chemicals were used as received. *p*-Aminophenyl-phosphate monosodium salt was purchased from LKT Lab Inc. or donated by Prof. Uichi Akiba of Akita University.

2.2. Cell culture and transfection

HeLa cells were donated by the Cell Resource Center for Biomedical Research (Tohoku University) and seeded at a density of 5×10^5 cells in RPMI-1640 medium containing 10% FBS, without antibiotics. After 1 day of culture, transfection was performed by addition of 500 μL Opti-MEM I medium containing 8×10^{-4} ng/μl plasmid and 10 μL Lipofectamine 2000 for 5 h. Subsequently, the transfection medium was changed to pure culture medium and the cells were incubated at 37 °C for 24 h. All plasmid DNA vectors including Luc (pGL3), GFP (pAcGFP-N1), and SEAP (pNFKB-SEAP) were purchased from Clontech and BD Sciences. HeLa-Luc-stable was established as described in the literature and donated by H. Akita, Hokkaido University [18]. The averaged *luc* gene copy number per cell at DNA level was 3. Single-cell CL imaging for HeLa-Luc-stable was not possible due to a relatively lower protein expression level.

2.3. Quantification of reporter protein based on chemiluminescence and fluorescence imaging

Luc and GFP protein expression activities from single cells were quantified with a CL and FL imaging system, respectively. CL imaging was performed with an inverted optical microscope (Olympus IX71) to which was attached a high-sensitivity CCD camera (Evolve 512; Photometrics) and image analysis software (Aquacosmos; Hamamatsu Photonics) in culture medium containing 500 μM luciferin. Cells showing CL intensity higher or lower than 10^4 counts per min were categorized as HeLa-pLuc(+CL) and HeLa-pLuc(−CL), respectively. Single-cell pick-up was subsequently performed on the same inverted microscope using a micromanipulator system. For FL imaging, an Hg lamp was used as the light source and fluorescence signals in culture medium were detected with a CCD camera (PD71; Olympus). Filter block (Ex, 450–490 nm; Em, 520 nm) was selected. Cells showing FL intensity higher and lower than 10^5 counts per 6 s were categorized as HeLa-pGFP(+FL) and HeLa-pGFP(−FL), respectively.

2.4. Electrochemical technique

SEAP protein expression was quantified using an electrochemical technique [19]. HeLa cells transfected with pNFKB-SEAP vector were incubated in 100 nM TNF-α for 24 h before being seeded on PDMS microwells (+TNF). As a control, the same transfected HeLa cells were incubated in culture medium (−TNF). The PDMS microwell array was fabricated by using a SU-8 master on a silicon wafer. The depth and diameter of the PDMS microwells were 30 μm. Medium containing cultured cells was poured over the PDMS microwell array. After the single cells were trapped in the microwells, the surface was rinsed with fresh medium to remove cells outside the microwell. Next, the single-cell array was placed in 3 mL of a measuring solution containing 1.0 mM PAPP and HEPES buffer (pH 9.5). A two-electrode system comprising a Pt microdisk, with a diameter of 20 μm, as the working electrode and an Ag/AgCl reference/counter electrode was used for electrochemical measurements. The position of the Pt microelectrode was controlled with a motor-driven XYZ positioner (Chuo-Seiki M9103). Chronoamperometric measurements for individual HeLa cells were performed on PDMS microwell to isolate the volume of the measuring solution surrounded by the walls of the microelectrode and the PDMS microwell [20]. The tip potential was maintained at 0.0 V for 1 min to accumulate the product, *p*-aminophenol (PAP), within the microwell. Then, the tip potential was stepped to 0.3 V to oxidize the PAP that accumulated in the microwell. The current response was converted to the electric charge (Q/nC) by time integration of the current and taken as protein activity. The response for the vacant microwell was subtracted as background.

2.5. Single-cell pick-up system

A glass capillary tube (1.5 mm o.d., 0.86 mm i.d.; Harvard Apparatus) was pulled with a capillary puller (model PN-3; Narishige) and cut with precision scissors to form a microcapillary tip with an outer diameter of 10–20 μm [13]. The surface of the microcapillary probe was modified with fluorosilane LS-912 (3,3,4,4,5,5,6,6,6-non-afluorohexyltrichlorosilane; Shin-etsu Chem. Ind. Co., Ltd.) by gas-phase silanization under a nitrogen atmosphere for 2 h at room temperature. The fluorosilane coating process was essential to prevent the adsorption of cytosol and nucleic acids on the inner/outer glass surface of the probe. Before use, the microcapillary probe was washed with 99.5% ethanol, dried, and exposed to UV irradiation on a clean bench (Oriental Giken Inc.) for more than 30 min. The microcapillary probe was used to pick single cells from a monolayer cultured in medium (RPMI-1640 or DMEM-F12) under observation with an Olympus IX71 microscope. The position of the probe was controlled using an oil-derived three-axis manual micromanipulator (MNO-203; Narishige). The capillary was exchanged for each single-cell pick up process. The single-cell pick-up operation was accomplished within 30 min after the CL, FL imaging or electrochemical evaluation.

2.6. Single-cell mRNA analysis

Collected solution with a volume of less than 1 μL and containing a single- or lysed cell was transferred into a 0.2 mL PCR tube. Lysis buffer (Lysis Buffer RLT from RNeasy Micro Kit; Qiagen) solution (75 μL) was further added to the PCR tube and vortexed. The RLT buffer functions to deactivate RNase and stabilize the RNA. Carrier RNA (Qiagen) (5 μL) was added in order to prevent the loss of the objective mRNA. Total RNA purification was performed according to the protocol for the RNeasy Micro Kit (Qiagen). The RT reaction was carried out to synthesize first-strand cDNA according to the protocol for the QuantiTect reverse transcription kit (Qiagen) at 42 °C for 30 min (RT reaction) followed by 95 °C for 3 min (deactivation of RTase). Synthesized cDNA sample solutions with a final volume of 20 μL were stored at −80 °C. qPCR was performed using the LightCycler 1.5 System (Roche) and the LightCycler Fast Start DNA Master kit (Roche) with a total volume of 20 μL in glass capillaries. Two microliters of a cDNA sample, 1.6 μL of 25 mM $MgCl_2$, 1 μL of 10 μM forward (Fw) primer, 1 μL 10 μM reverse (Rv) primer, 2 μL of SYBR Green, and 12.4 μL of H_2O were added. After initial denaturation at 95 °C for 10 min, 45

PCR cycles were performed with denaturation at 95 °C for 10 s, annealing at the annealing temperature of the individual primer pair as mentioned below for 10 s, and extension at 72 °C for 9 s. Primers for glyceraldehyde-3-phosphate dehydrogenase (GAPDH;

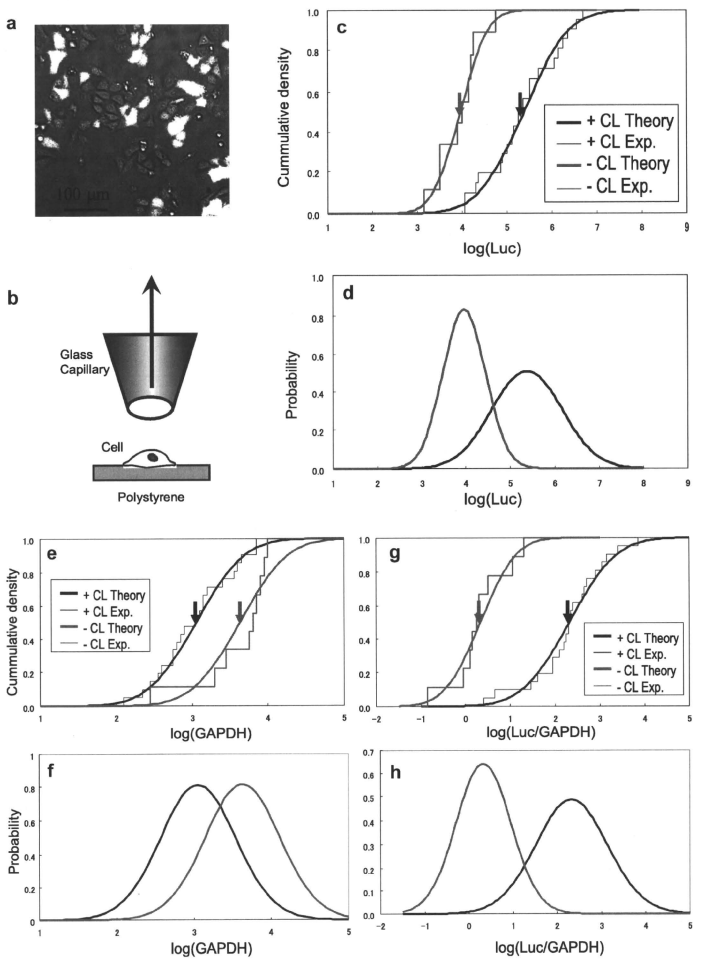

Fig. 1. (a) CL image, the color of which does not reflect the wavelength of Luc emission, overlaid on an optical image of HeLa cells transfected with pGL3 vector. Transfected HeLa cells were categorized as having significant chemiluminescence, +CL or no luminescence, −CL. Scale bar, 100 μm. (b) Single cells were collected using the capillary suction method. (c–h) Cumulative rates as a function of log (Luc), log (GAPDH), and log (Luc/GAPDH). The absolute mRNA copy numbers of Luc and GAPDH were determined by RT-qPCR. Solid and gray lines indicate +CL and −CL, respectively. Theoretical lognormal distribution curves (probability function; d, f, h) and their accumulation (cumulative density function; c, e, g) were derived from the experimentally obtained mean and S.D. values listed in Table 1. Arrows indicate mean on a logarithmic scale. c and g, $P < 0.001$; e, $P = 0.007$; *t*-test. Variances of the distribution were identical due to $P = 0.08$, 0.52, and 0.21 for c, e, and g; *F*-test.

GenBank Accession No. M33197), firefly luciferase (Luc; Genbank Accession No. U47123), green fluorescent protein (GFP; Accession No. AY151052), and secreted alkaline phosphatase (SEAP, Genbank Accession No. U89938) were designed and synthesized by Nihon Gene Research Laboratories Inc. The actual sequences, amplicon sizes, and annealing temperatures of the primers were as follows. GAPDH (Fw) 5′-TGAACGGGAAGCTCACTGG-3′, (Rv) 5′-TCCACCACCCTGTTGCTGTA-3′, 307 bp, 62 °C; Luc (Fw) 5′-GGT CCT ATG ATT ATG TCC GGT TAT-3′, (Rv) 5′-ATG TAG CCA TCC ATC CTT GTC AAT-3′, 78 bp, 62 °C; GFP (Fw)5′-CCG ACC ACT ACC AGC AGA A-3′, (Rv) 5′-GGT CAC GAA GCC GAA GTA-3′, 140 bp, 60 °C; SEAP (Fw) 5′-TTC GAG CAG ACA TGA TAA GA-3′, (Rv) 5′-GCA ATA GCA TCA CAA TTT CAC-3′, 100 bp, 60 °C. The copy number of cDNA from single-cell samples was estimated from the calibration curve for the standard DNA sample encoding GAPDH, Luc, GFP, and SEAP. The calibration curves are shown in Supplementary data (Fig. S1). For the four genes, the linearities of the calibration curves were excellent and the PCR efficiencies were all in the range of 95–100%. Standard samples to estimate mRNA copy number for GAPDH, Luc, and GFP were synthesized by Nihon Gene Research Laboratories Inc. For SEAP, plasmid vector pSEAP2-Control (Clontech, BD Biosciences) was used as received.

3. Results

Luc was transiently introduced into HeLa cells by the use of a commercially available plasmid vector encoding CMV promoter upstream of the firefly Luc gene. We investigated mRNA and protein expression as a function of time after lipofection, and found that mRNA expression reached maximum 12–24 h after lipofection and became almost zero 7 days after lipofection. Luc mRNA can be synthesized without stimulation, but the vector itself is lost from the cell during the passage process. The CL intensity from individual cells, 24 h after lipofection, was recorded as an indicator of protein expression activity with a high-sensitivity CCD camera and image analysis software (Fig. 1(a)). Cells with CL intensity higher and lower than 10^4 counts per min were categorized as HeLa-pLuc(+CL) and HeLa-pLuc(−CL), respectively. Subsequently, the cells were picked up with a capillary probe connected to a disposable syringe (Fig. 1(b)). Each single cell collected was placed in a PCR tube filled with cell lysis buffer, after which RT-qPCR was performed.

Fig. 1(c) shows cumulative frequency curves as a function of $\log_{10}$ (Luc mRNA copy number) for HeLa-pLuc(+CL) and HeLa-pLuc(−CL) cells. The theoretical cumulative frequency curves (Fig. 1(c), overlaid) and relative frequency curves (probability function, Fig. 1(d)) for the lognormal distribution were also derived by introducing the mean and standard deviation (S.D.), obtained experimentally, on a logarithmic scale of the individual data points. The histograms of internally expressed GAPDH and relative Luc expression normalized to GAPDH were in good agreement with the lognormal distribution (Fig. 1(e–h)). Important parameters obtained for all experimental conditions in this study, including the arithmetic mean (μ_{Art}) and geometric mean (μ_{Geo}), are listed in Table 1. The mean S.D. and skewness were expressed on a logarithmic scale and used to obtain theoretical lognormal distribution curves.

For +CL and −CL cells, the experimental and theoretical results were in very good agreement. The F value was small enough to assume identical variance of the two distributions ($F = (s_1/s_2) = 2.66$, $P = 0.08$, where s_1 and s_2 are the variances of +CL and −CL, respectively). There was a significant difference in the mean value

Table 1
Parameters obtained for all experimental conditions in this study, including sample number (N), arithmetic mean (μ_{Art}) and geometric mean (μ_{Geo}). Mean, S.D., and skewness are shown on a logarithmic scale and were used to obtain theoretical lognormal distribution curves.

Category	Gene	N	μ_{Arth}	μ_{Geo}	Mean	S.D.	S.D./mean	Skewness
Luc								
pLuc(+CL)	GAPDH	21	2014	1136	3.0553	0.4932	0.1614	0.0456
	Luc	21	858 932	237 572	5.3758	0.7855	0.1461	−0.0097
	Luc/GAPDH	21	807	209	2.3205	0.8211		−0.5367
	Protein	21	1947 648	931 059	5.9690	0.5535	0.0927	0.1122
pLuc(−CL)	GAPDH	9	5988	4265	3.6299	0.4903	0.1351	−1.9172
	Luc	9	15 219	9135	3.9607	0.4815	0.1216	−0.0484
	Luc/GAPDH	9	4.82	2.14	0.3308	0.6227		−0.2324
Luc-stable (1-cell pick)	GAPDH	11	1514	937	2.9719	0.4810	0.1618	−0.4173
	Luc	11	650	416	2.6195	0.5265	0.2010	−1.3540
	Luc/GAPDH	11	1.29	0.44	−0.3525	0.7791		−0.8589
Luc-stable (4-cell pick)	GAPDH	8	1605	1402	3.1469	0.2530	0.0804	−0.6126
	Luc	8	772	627	2.7973	0.3098	0.1108	−0.3853
	Luc/GAPDH	8	0.48	0.45	−0.3496	0.1912		−0.8256
Non-Cell	GAPDH	6	10 432	10 364	4.0155	0.0542	0.0135	0.3631
	Luc	6	14 193	14 031	4.1471	0.0721	0.0174	−0.0534
GFP								
pGFP (+FL)	GAPDH	18	3954	1240	3.0933	0.6613	0.2138	0.5581
	GFP	18	24 233	5635	3.7509	0.8074	0.2153	0.1692
	GFP/GAPDH	18	20.05	4.55	0.6576	0.8580		0.0019
	Protein	18	757 742	680 163	5.8326	0.2113	0.0362	−0.2112
pGFP (−FL)	GAPDH	20	1798	1175	3.0699	0.4190	0.1365	0.0230
	GFP	20	814	217	2.3355	0.7486	0.3205	0.4407
	GFP/GAPDH	20	1.92	0.18	−0.7344	0.9257		0.5995
SEAP								
pNFkB-SEAP (+TNF)	GAPDH	8	911	785	2.8950	0.2700	0.0933	−0.7544
	SEAP	8	4599	2866	3.4573	0.4048	0.1171	1.2511
	SEAP/GAPDH	8	4.63	3.65	0.5623	0.3088		0.5268
	Protein	8	5.15	4.51	0.6543	0.2827	0.4321	−2.0951
pNFkB-SEAP (−TNF)	GAPDH	7	3140	2793	3.4461	0.2303	0.0668	−0.0546
	SEAP	7	2610	1851	3.2673	0.3945	0.1207	0.2282
	SEAP/GAPDH	7	1.26	0.66	−0.1788	0.5267		0.5368
	Protein	7	2.41	1.54	0.1881	0.4612	2.4514	0.2232

Note: $\mu_{Art} = \frac{1}{N}\sum_{i=1}^{N} x_i$, $\mu_{Geo} = (\prod_{i=1}^{N} x_i)^{1/N}$, Mean $= \frac{1}{N}\sum_{i=1}^{N} (\log x_i)$, skewness indicates a measure of the asymmetry of the probability function [9].

($P < 0.001$, t-test). We believe this result is important because we found a statistical difference in mRNA copy number per cell between the two sorted groups based on protein expression (+CL and −CL). Thus, there was a correlation between mRNA and protein expression at the single-cell level. This should be borne in mind when reading a later section of this article, where we show that

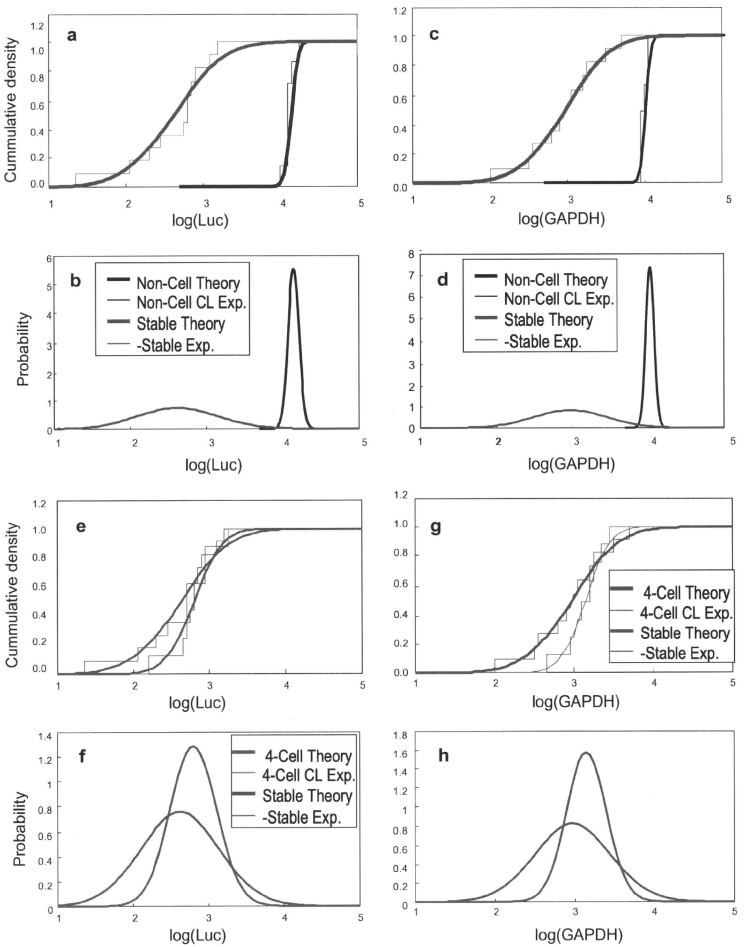

Fig. 2. (a–d) Cumulative rates as a function of log (Luc) and log (GAPDH) from a non-cell sample (solid line) and one HeLa-Luc-stable cell (gray line). Theoretical lognormal distribution curves (b and d) and their accumulation (a and c) were derived from experimentally obtained mean and S.D. values listed in Table 1. (e–h) Cumulative rates as a function of log (Luc) and log(GAPDH) from four-cell pick-up of HeLa-Luc-stable (solid line) and one-cell pick-up of HeLa-Luc-stable (gray line). Variances of the distribution were evaluated by F-test: a and c, $P < 0.001$; e and g, $P = 0.09$ and 0.05, respectively.

the correlation coefficient (R) between mRNA and protein expression at the single-cell level was much lower than 1.00.

In the following experiments we used a HeLa strain stably expressing Luc, HeLa-Luc-stable [18]. HeLa-Luc-stable is a strain that maintains CL activity during passage because Luc is inserted in the genomic DNA of the host cell. In HeLa-Luc-stable cells, Luc is continuously expressed in the absence of any stimulus. Real-time PCR was also carried out in a non-cellular system to establish that noise from single-cell experiments could be clearly distinguished amongst the noise from PCR instruments and operation. A DNA standard sample was prepared to contain the same amount of DNA as a single cell (0.3 μL volume of a non-cell sample containing GAPDH and Luc at concentrations of 5.0×10^4 copies/μL). The non-cell sample was collected with a glass capillary probe, and the protocol was the same as that used for the single-cell analysis. As expected, the distributions of Luc and GAPDH from the non-cell sample were very narrow compared with those from single cells (Fig. 2(a–d)). The F values were very large ($F = (s_1/s_2) = 53$, $P < 0.001$ for Luc and $F = 79$, $P < 0.001$ for GAPDH, where s_1 and s_2 are the variances for single-cell and non-cell samples, respectively) and the variances were not statistically identical. This result clearly demonstrates that the noise level from the PCR instruments and operations can be separated with ease from the fluctuation of mRNA expression in single cells.

Next, our single-cell analysis procedure was used for more than two cells. In this experiment, two to four cells were picked up with a single capillary suction device and then cDNA synthesis and qPCR were performed. Again, the width of the curve obviously became narrow (Fig. 2(e–h)). The F value was large ($F = (s_1/s_2) = 2.89$, $P = 0.09$ for Luc and $F = 3.61$, $P = 0.05$ for GAPDH, where s_1 and s_2 indicate the distribution for single-cell and four-cell pick-up, respectively), although the difference in variance was not statistically significant. Previous studies indicated that the fluctuations decreased as the number of cells picked increased [12,13,15].The mean values of mRNA copy number for single-cell and four-cell experiments, normalized by cell number, were in very good agreement.

Because we performed absolute quantification of mRNA copy number from single cells, it is also possible to discuss the differences in variance between the Luc and GAPDH genes. Interestingly, the variances of Luc (s_1) and GAPDH (s_2) were statistically different for HaLa-pLuc (+Luc) ($F = (s_1/s_2) = 2.54$, $P = 2.2 \times 10^{-2}$), whereas the variances were identical for HeLa-pLuc (−Luc) ($F = 0.96$, $P = 0.48$) and HeLa-Luc-stable ($F = 1.20$, $P = 0.39$). The Luc mRNA copy number for transiently transformed cells (HeLa-pLuc (+Luc)) appeared to have a very wide distribution compared with Luc mRNA for the stable cell line, HeLa-Luc-stable and the internally expressed GAPDH mRNA. Expression of mRNA with copy number greater than 10^5 per cell is only possible by artificially introducing external genes using vectors.

Fig. 3 shows logarithmic plots of chemical luminescence output log (protein) versus log (Luc mRNA), log (GAPDH mRNA), and log (Luc/GAPDH). The R values for the linear plot versus Luc, GAPDH, and (Luc/GAPDH) were 0.52, −0.17, and 0.76, respectively, and the R values for the corresponding logarithmic plots were 0.35, −0.15, and 0.43, respectively. It is noteworthy that the R value for GAPDH was much smaller than that for Luc. This is reasonable because GAPDH mRNA is only slightly related to Luc protein expression. The R value for (Luc/GAPDH) was identical to that for Luc, and elevation of the noise level was not observed when the Luc mRNA copy number was normalized to GAPDH. In the above section, we focused on the Luc reporter system and pointed out several significant findings. (1) mRNA copy number per cell ranging 10^3 to 10^7 showed a lognormal distribution for both externally introduced reporter genes and internally expressed genes. (2) The R value between mRNA and protein expression at the single-cell level was much lower than 1.00.

We verified these findings with other reporter systems, GFP and SEAP. GFP was transiently introduced into HeLa cells by the use of plasmid vector pAcGFP-N1. Cells showing an FL intensity higher or lower than 10^5 counts per 6 s were categorized as HeLa-pGFP(+FL) and HeLa-pGFP(−FL), respectively. The results are shown in Fig. 4(a and b), together with microscopic images. Cumulative frequency curves as a function of GFP, GAPDH, and GFP/GAPDH are shown on a logarithmic scale (Fig. 4(c) and Supplementary data Fig. S2). Theoretical cumulative frequency and relative frequency curves were also derived by assuming the experimentally obtained mean and S.D. values (see Table 1). The results obtained for the GFP system were qualitatively the same as those obtained for the Luc system. Plots of log (protein) versus log (GFP mRNA), versus log (GAPDH mRNA), and versus log (GFP/GAPDH) are shown in Supplementary data Fig. S3. The R values for the linear plot versus GFP, GAPDH, and (Luc/GAPDH) were 0.14, −0.25, and 0.21, respectively, and the R values for the corresponding logarithmic plots were 0.10, −0.098, and 0.17, respectively. We also found that the slope of the line obtained by the minimum square method for the reporter protein versus the reporter mRNA copy number was much larger (often with the opposite sign) than the slope of the reporter protein versus mRNA copy number of the internally expressed gene, for both Luc and GFP (Figs. 3 and S3).

Finally, cellular signal transduction was monitored as mRNA and protein expression at the single-cell level. We selected the NFκB pathway as a model, in which the NFκB protein complex binds to the κB element, triggering transcription of genes down-

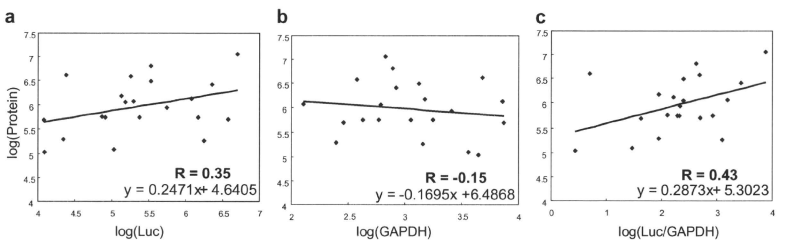

Fig. 3. Logarithms of CL output log (protein) versus log (Luc mRNA), log (GAPDH mRNA) and log (Luc/GAPDH). R for Luc, GAPDH, and (Luc/GAPDH) was 0.35, −0.15, and 0.43, respectively.

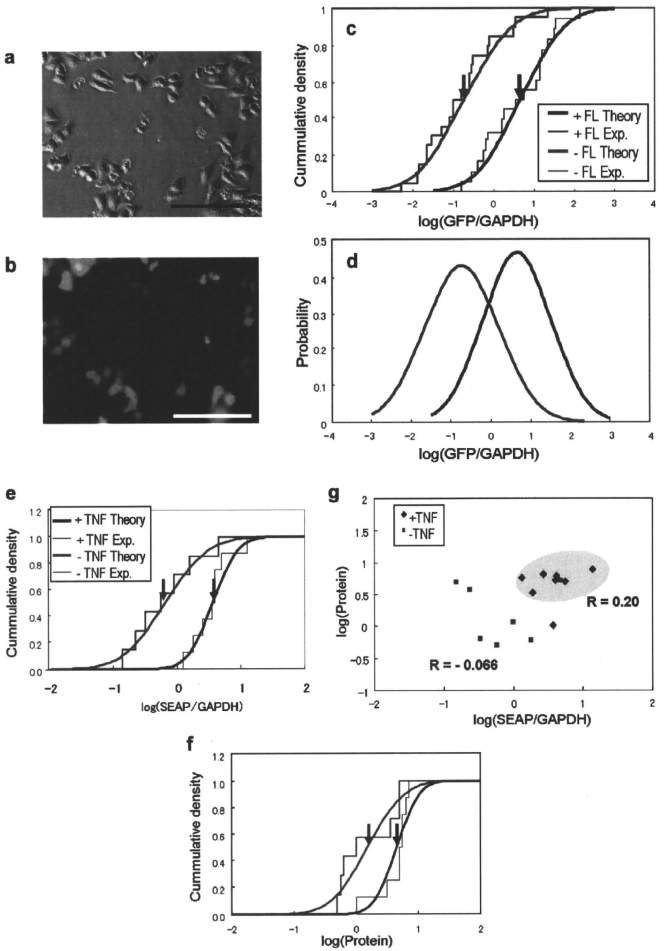

Fig. 4. (a and b) FL and optical images of HeLa cells transfected with pAcGFP-N1 vector. Transfected HeLa cells were categorized as showing significant fluorescence, +FL, or no fluorescence, −FL. Scale bars, 100 μm. (c and d) Cumulative rates as a function of log (GFP/GAPDH). The absolute mRNA copy numbers of GFP and GAPDH were determined using RT-qPCR. Solid and gray lines indicate +FL and −FL, respectively. (e and f) Cumulative rates as a function of log (SEAP/GAPDH) and log (protein) from HeLa-pNFKB-SEAP cells incubated with TNF-α (+TNF, solid line) and negative control (−TNF, gray line). Theoretical lognormal distribution curves and their accumulation were derived from the experimentally obtained mean and S.D. values listed in Table 1. (g) Log (protein) versus log (SEAP/GAPDH) for +TNF (diamond) and −TNF (square). *R* values for +TNF and −TNF Luc were 0.20 and −0.066, respectively. SEAP reporter protein activity was evaluated electrochemically. Arrows indicate the mean on a logarithmic scale. c, $P < 0.001$; e, $P = 0.005$; f, $P = 0.03$; *t*-test. Variances of the distribution were identical due to $P = 0.38$, 0.09, and 0.11 for c, e, and f; *F*-test.

stream of the promoter region [19,20]. HeLa cells were transfected with the plasmid vector pNFκB-SEAP (HeLa–pNFκB-SEAP), and secreted SEAP upon stimulation with a cytokine such as TNF-α. Fig. 4(e and f) shows the lognormal cumulative plots and theoretical curves as a function of log (SEAP/GAPDH) before and 24 h after stimulation with TNF-α. The relative expression of SEAP mRNA normalized to GAPDH after TNF-α stimulation was statistically greater than that before stimulation ($P < 0.001$, t-test). Electrochemical responses were evaluated as SEAP reporter protein expression activity [21–23]. Fig. 4(g) shows log (protein) versus log (SEAP/GAPDH). The R value for the logarithmic plot was 0.20 and −0.066 for +TNF and −TNF, respectively. This result suggests that cellular signal transduction can be monitored from single cells because of transcription and protein levels.

4. Discussion

We focused on verifying whether stochastic nature in single cell system was still observed or not for an extremely higher mRNA expression activity with 10^7 copies per cell. HeLa cells transfected with several plasmid vectors were used as a model single-cell system (HeLa-pLuc, HeLa-pGFP), because a high transcription activity with mRNA copy number greater than 10^5 per cell is only possible by artificially introducing external genes using vectors. In our experiment, HeLa strain stably expressing Luc (HeLa-Luc-stable) and non-cell sample were also investigated with the same experimental system. A logarithmic plot [9,10] of the fluctuating mRNA copy number from single-cell analysis was found to be very powerful and widely applicable, allowing statistical comparison of variances (F-test) and means (t-test) and evaluation of the correlation between different genes and hierarchical relations between transcriptional and translational activity at the single-cell level. A lognormal distribution of the number of mRNA molecules within a cell was valid not only for internally expressed genes but also for externally introduced genes with 10^7 copies per cell. This is an unexpected finding because it has been assumed that a relatively small number of molecules ($<10^3$) of mRNA or protein within the cell generate fluctuations during the gene expression process, including translation and transcription, in most mathematical models used for single-cell noise analysis [4–8]. From the technical point of view, direct counting of the number of mRNA molecules was performed based on FISH [7]; however, it is very difficult to quantify more than 10^3 copies of mRNA molecules. PCR-based mRNA analysis will provide information about single-cell gene expression analysis with a much wider dynamic range, although it is necessary to separate the noise from the noise associated with the instrument and operation.

Recently, global-scale gene expression analysis has become possible in bulk experiment ($>10^3$ cells), to quantify almost all kinds of mRNA and protein expressed in bacteria, yeast and mammalian cells [8,24–27]. In these studies, mRNA versus protein plots in logarithmic scale were performed. The correlation between the mRNA and protein was found to be very poor. This result is explained by molecular scale non-linear mechanisms including the delay between the transcription of mRNA and the translation of protein, the differences in degradation rates for mRNA and proteins, and the number of protein molecules synthesized from a single mRNA molecule.

In bulk experiment ($>10^3$ cells) utilizing reporter system such as Luc and GFP, the expression levels of mRNA and protein were well correlated as far as the time scale monitoring protein expression was sufficiently long. This experiment is different from the global-scale gene expression analysis because only one type of reporter system was monitored at mRNA and protein levels. The delay between the transcription of mRNA and the translation of protein, the differences in degradation rates for mRNA and proteins, and the number of protein molecules synthesized from a single mRNA molecule are all smoothed because very large number of mRNA and protein molecules were concerned. For example, in the GFP reporter system, used in this study as a model protein with a relatively larger half life ($t_{1/2} = \sim 24$ h) [28–30], the expression levels of mRNA and protein were well correlated: When increasing the plasmid vector concentration during the lipophection process, expression levels of mRNA and protein increased. As we showed in Figs. 1, 4 and S2, the copy numbers of mRNA per cell between +CL ($N = 21$) and −CL ($N = 9$), between +FL ($N = 18$) and −FL ($N = 20$) were statistically distinguishable.

Raj et al. investigated the correlation between mRNA and protein expressions of GFPs in the linear plots at single-cell level [7]. According to their theoretical calculation based on a random transition model, the R value becomes smaller with increasing $t_{1/2}$: proteins with $t_{1/2}$ of 1.56, 25, and 200 h showed R values of 0.92, 0.43, and 0.17, respectively. The $t_{1/2}$ for Luc and SEAP were very short (~2 h) comparing to that for GFP [30,31]. Taken together, it was suggested that our results might be supported by the theoretical calculation that the small R values reflected a relatively longer half-life of reporter proteins, because the R for Luc was slightly larger than that for GFP. The poor correlations between the mRNA and the protein expressions at single-cell level observed in this study and reported by Raj et al. [7] reflects the stochastic events occurring in single-cell, even though the mRNA copy number per cell in our experiment (10^7) and Raj et al. ($<10^3$) were different. Previous studies and Fig. 2(e–h) indicated that the fluctuations decreased as the number of cells picked increased [12,13,15] whereas the increase in the mRNA copy number per cell did not contribute to decline the gene expression fluctuation.

In conclusion, mRNA from single cells was quantified using real-time RT-PCR after recording the address and reporter protein activity with CL, FL, and electrochemical techniques, using Luc, GFP, and SEAP. mRNA copy number per cell ranging 10^3 to 10^7 showed a lognormal distribution for both externally introduced reporter genes and internally expressed genes. We succeeded to extend the applicability of single-cell analysis system to detect very high copy number of mRNA. The fluctuations in the gene expression was decreased as increasing the number of cells picked but not decreased as increasing mRNA copy number per cell. The R value between mRNA and protein expression at the single-cell level was much lower than 1.00, which might reflect the degradation rate of the reporter proteins.

Acknowledgement

This work was partly supported by a Grant-in-Aid for Scientific Research on Priority Areas (17066002) "Life Surveyor" from MEXT, of Japan; by a Grant-in-Aid for Scientific Research (18101006, 21685008, and 21106502) from MEXT; and by a grant from the Center for Interdisciplinary Research, Tohoku University.

Appendix A. Supplementary data

Supplementary data associated with this article can be found, in the online version, at doi:10.1016/j.febslet.2010.08.008.

References

[1] Chang, H.H., Hemberg, M., Barahona, M., Ingber, D.E. and Huang, S. (2008) Transcriptome-wide noise controls lineage choice in mammalian progenitor cells. Nature 453, 544–547.
[2] Stahlberg, A., Bengtsson, M., Hemberg, M. and Semb, H. (2009) Quantitative transcription factor analysis of undifferentiated single human embryonic stem cells. Clin. Chem. 55, 2162–2170.
[3] Toyooka, Y., Shimamoto, D., Murakami, K., Takahashi, K. and Niwa, H. (2008) Identification and characterization of subpopulations in undifferentiated ES cell culture. Development 135, 909–918.

[4] Elowitz, M.B., Levine, A.J., Siggia, E.D. and Swain, P.S. (2002) Stochastic gene expression in a single cell. Science 297, 1183–1186.
[5] Ozbudak, E.M., Thattai, M., Kurtser, I., Grossman, A.D. and van Oudenaarden, A. (2002) Regulation of noise in the expression of a single gene. Nat. Genet. 31, 69–73.
[6] Raser, J.M. and O'Shea, E.K. (2004) Control of stochasticity in eukaryotic gene expression. Science 304, 1811–1814.
[7] Raj, A., Peskin, C.S., Tranchina, D., Vargas, D.Y. and Tyagi, S. (2006) Stochastic mRNA synthesis in mammalian cells. PLoS Biol. 4, e309.
[8] Williamson, A.J.K., Smith, D.L., Blinco, D., Unwin, R.D., Pearson, S., Wilson, C., Miller, C., Lancashire, L., Lacaud, G., Kouskoff, V. and Whetton, A.D. (2008) Quantitative proteomics analysis demonstrates post-transcriptional regulation of embryonic stem cell differentiation to hematopoiesis. Mol. Cell Proteomics. 7, 459–472.
[9] Bengtsson, M., Stahlberg, A., Rorsman, P. and Kubista, M. (2005) Gene expression profiling in single cells from the pancreatic islets of Langerhans reveals lognormal distribution of mRNA levels. Genome Res. 15, 1388–1392.
[10] Warren, L., Bryder, D., Weissman, I.L. and Quake, S.R. (2006) Transcription factor profiling in individual hematopoietic progenitors by digital RT-PCR. Proc. Natl. Acad. Sci. USA 103, 17807–17812.
[11] Zhong, J.F., Chen, Y., Marcus, J.S., Scherer, A., Quake, S.R., Taylor, C.R. and Weiner, L.P. (2008) A microfluidic processor for gene expression profiling of human embryonic stem cells. Lab Chip 8, 68–74.
[12] Taniguchi, K., Kajiyama, T. and Kambara, H. (2009) Quantitative analysis of gene expression in a single cell by qPCR. Nat. Methods 6, 503–506.
[13] Nashimoto, Y., Takahashi, Y., Yamakawa, T., Torisawa, Y.S., Yasukawa, T., Ito-Sasaki, T., Yokoo, M., Abe, H., Shiku, H., Kambara, H. and Matsue, T. (2007) Measurement of gene expression from single adherent cells and spheroids collected using fast electrical lysis. Anal. Chem. 79, 6823–6830.
[14] Shiku, H., Yamakawa, T., Nashimoto, Y., Takahashi, Y., Torisawa, Y.S., Yasukawa, T., Ito-Sasaki, T., Yokoo, M., Abe, H., Kambara, H. and Matsue, T. (2009) A microfluidic dual capillary probe to collect messenger RNA from adherent cells and spheroids. Anal. Biochem. 385, 138–142.
[15] Hong, J.W., Studer, V., Hang, G., Anderson, W.F. and Quake, S.R. (2004) A nanoliter-scale nucleic acid processor with parallel architecture. Nat. Biotechnol. 4, 435–439.
[16] Gibson, J.D., Jaktuba, C.M., Boucher, N., Holbrook, K.A., Carter, M.G. and Nelson, C.E. (2009) Single-cell transcript analysis of human embryonic stem cells. Integr. Biol. 1, 540–551.
[17] Janes, K.A., Wang, C.-C., Holmberg, K.J., Cabral, K. and Brugge, J.S. (2010) Identifying single-cell molecular programs by stochastic profiling. Nat. Methods 7, 311–317.
[18] Masuda, T., Akita, H., Nishio, T., Niikura, K., Kogure, K., Ijiro, K. and Harashima, H. (2008) Development of lipid particles targeted via sugar-lipid conjugates as novel nuclear gene delivery system. Biomaterials 29, 709–723.
[19] Murata, T., Yasukawa, T., Shiku, H. and Matsue, T. (2009) Electrochemical single-cell gene-expression assay combining dielectrophoretic manipulation with secreted alkaline phosphatase reporter system. Biosens. Bioelectron. 25, 913–919.
[20] Shiku, H., Suzuki, J., Murata, T., Ino, K., Matsue, T. (in press) Chronoamperometric characterization of secreted alkaline phosphatase from single cell entrapped in a poly(dimethylsiloxane) microwell. Electrochim. Acta. doi:10.1016/j.electacta.2010.04.011.
[21] Torisawa, Y.S., Ohara, N., Nagamine, K., Kasai, S., Yasukawa, T., Shiku, H. and Matsue, T. (2006) Electrochemical monitoring of cellular signal transduction with a secreted alkaline phosphatase reporter system. Anal. Chem. 78, 7625–7631.
[22] Lin, Z., Takahashi, Y., Murata, T., Takeda, M., Ino, K., Shiku, H. and Matsue, T. (2009) Electrochemical gene-function analysis for single-cells with addressable microelectrode/microwell arrays. Angew. Chem. Int. Ed. 48, 2044–2046.
[23] Takahashi, Y., Shiku, H., Murata, T., Yasukawa, T. and Matsue, T. (2009) Transfected single-cell imaging by scanning electrochemical optical microscopy with shear force feedback regulation. Anal. Chem. 81, 9674–9681.
[24] Ghaemmaghami, S., Huh, W.-K., Bower, K., Howson, R.W., Belle, A., Dephoure, N., O'Shea, E.K. and Weissman, J.S. (2003) Global analysis of protein expression in yeast. Nature 425, 737–741.
[25] Hayashi, A., Da-Qiao, D., Tsutsumi, C., Chikashige, Y., Masuda, H., Haraguchi, T. and Hiraoka, Y. (2009) Localization of gene products using a chromosomally tagged GFP-fusion library in the Fission yeast *Schizosaccharomyces pombe*. Genes Cells 14, 217–225.
[26] Matsuyama, A., Arai, R., Yashiroda, Y., Shirai, A., Kamata, A., Sekido, S., Kobayashi, Y., Hashimoto, A., Hamamoto, M., Hiraoka, Y., Horinouchi, S. and Yoshida, M. (2006) ORFeome cloning and global analysis of protein localization in the fission yeast *Schizosaccharomyces pombe*. Nat. Biotechnol., 24, 841–847.
[27] Ishii, N., Nakahigashi, K., Baba, T., Robert, M., Soga, T., Kanai, A., Hirakawa, T., Naba, M., Hirai, K., et al. (2007) Multiple high-throughput analysis monitor the response of *E. coli* to perturbations. Science 316, 593–597.
[28] Corish, P. and Tyler-Smith, C. (1999) Attenuation of green fluorescent protein half-life in mammalian cells. Protein Eng. 12, 1035–1040.
[29] Chalfie, M., Tu, Y., Euskirchen, G., Ward, W.W. and Prasher, D.C. (1994) Green fluorescent protein as a marker for gene expression. Science 263, 802–805.
[30] Li, X., Zhao, X., Fang, Y., Jiang, X., Duong, T., Fan, C., Huang, C.-C. and Kain, S.R. (1998) Generation of destabilized green fluorescent protein as a transcription report. J. Biol. Chem. 273, 34970–34975.
[31] Thompson, J.F., Hays, L.S. and Lloyd, D.B. (1991) Modulation of firefly lucifarase and impact of studies of gene regulation. Gene 103, 171–177.

Electrochimica Acta 55 (2010) 8263–8267

Contents lists available at ScienceDirect

Electrochimica Acta

journal homepage: www.elsevier.com/locate/electacta

Chronoamperometric characterization of secreted alkaline phosphatase from single-cell entrapped in a poly(dimethylsiloxisane) microwell

Hitoshi Shiku*, Junya Suzuki, Tatsuya Murata, Kosuke Ino, Tomokazu Matsue*

Graduate School of Environmental Studies, Tohoku University, Aramaki Aoba 6-6-11, Sendai 980-8579, Japan

ARTICLE INFO

Article history:
Received 18 December 2009
Received in revised form 15 March 2010
Accepted 2 April 2010
Available online 10 April 2010

Keywords:
Scanning electrochemical microscopy
Alkaline phosphatase
Single-cell analysis
Poly(dimethylsiloxisane)

ABSTRACT

Single-cell analysis has become a powerful method to construct a new type of whole cell sensor integrating with individual cellular responses all together. However, sensitivity of electrochemical detection system in the present stage is insufficient to discuss in detail about the results obtained from a large number of data set because the individual single-cell responses are largely fluctuated. To improve sensitivity, chronoamperometry (CA) and electric charge analysis were performed for a single-cell entrapped within a poly(dimethylsiloxisane) (PDMS) microwell. HeLa cells transfected with vectors encoding SEAP (secreted alkaline phosphatase) have been seeded in the cylindrical PDMS microwell arrays with and without groove. A microelectrode tip located the top of the PDMS microwell to isolate the volume of the measuring solution containing *p*-aminophosphate (PAPP) as an enzymatic substrate. After a certain time period (t_{accu}) to promote the SEAP reaction, the tip potential was stepped from 0.0 to 0.3 V and the CA response for oxidation of *p*-aminophenol (PAP) was converted to the electric charge by time integration of the current. The electrochemical response from HeLa cells transfected with SEAP (HeLa-SEAP) was significantly larger than that from wild-type HeLa for both the PDMS microwell with and without groove. For the PDMS microwell without groove, accumulation of PAP was evidently observed with increasing t_{accu}. For the PDMS microwell with a groove of 5 μm width and 5 μm depth, the PAP oxidation current was large, but the accumulation of PAP was not evident with increasing t_{accu}, due to the promoted mass transfer of PAP and electric connection according to the groove.

1. Introduction

Recently, single-cell analysis has become focus of attention to provide new insight of cellular biology. It is now recognized that individual cells behave with a large diversity in gene expression activity at both transcription and translation levels even among a clonal population [1–3]. Single-cell experiments have been performed utilizing flow cytometry [1,2], fluorescence imaging [1], and mRNA analysis [4–7]. Among them, reporter protein system is especially appropriate to monitor the spatial and temporal fluctuations occurring at the single-cell level [1,8,9]. Evaluation of cellular signal pathways and detection of various ligand analytes are possible by combining the reporter system and a series of responsive elements encoded at specific DNA sequences.

Until now, HeLa cells transfected with vectors encoding secreted alkaline phosphatase (HeLa-SEAP) cell line is the only one that allows electrochemical single-cell gene expression analysis [10–15]. Electrochemical responses from 10 × 10 single-cell array were acquired within 22 s with our addressable microelectrode array device on which redox cycling at the crossing points of the column and row micro-band electrodes were sequentially detected [12]. In the present stage, however, the amperometric response from single-cell is so small (several pA) and therefore improvement on sensitivity is certainly required. To improve sensitivity, chronoamperometry (CA) and electric charge analysis were performed for a single-cell entrapped within a poly(dimethylsiloxane) (PDMS) microwell in this study. HeLa cells transfected with vectors encoding SEAP (secreted alkaline phosphatase) have been seeded in the cylindrical PDMS microwell arrays with and without groove. Previously, we have introduced electrochemical microanalysis system utilizing PDMS microwell array to characterize transfected yeast at cell number of hundreds level [16]. Microelectrode was used to cover the top of the cylindrical PDMS microwell, accumulate the product of enzyme reaction within the confined space, and convert the enzymatic product PAP amounts into electric charge, namely time integration of Faradaic current.

The cylindrical PDMS microwell is suitable for electrochemical single-cell analysis with a high-throughput manner because the distance between the sample and the detector electrode is strictly defined by the depth of the well. However, when the top of the PDMS microwell was covered with a microelectrode tip, it was

* Corresponding authors.
E-mail addresses: shiku@bioinfo.che.tohoku.ac.jp (H. Shiku), matsue@bioinfo.che.tohoku.ac.jp (T. Matsue).

0013-4686/$ – see front matter © 2010 Elsevier Ltd. All rights reserved.
doi:10.1016/j.electacta.2010.04.011

found that solution resistance in the experimental system originating from the leaky electric connection was not constant [16]. Consequently, a PDMS microwell with groove to promote electric connection was designed. We compared the electrochemical responses from single-cells entrapped within the PDMS microwell arrays with and without groove and discussed their advantages and disadvantages in the present study.

2. Experimental

2.1. Chemicals and materials

p-Aminophenol (PAP; Wako Pure Chemical Industries), 3,3,4,4,5,5,6,6,6-nonafluorohexyl trichlorosilane (LS-912; Shin-Etsu Chemical Co. Ltd.), 2-[4-(2-hydroxyethyl)-1-piperazinyl] ethanesulfonic acid (HEPES; Dojindo Laboratories, Japan), SU-8 (Microchem), SU-8 developer (Microchem), RPMI-1640 (Gibco Invitrogen, Tokyo, Japan), fetal bovine serum (FBS; Gibco), penicillin/streptomycin (Gibco), phosphate buffered saline (PBS(−); Wako Pure Chemical Industries), calcein-acetoxymethyl ester (calcein-AM; Dojindo Laboratories), propidium iodide (PI; Dojindo Laboratories), Opti-MEM I medium (Gibco), Lipofectamine™ 2000 (Invitrogen), and other chemicals were used as received. SEAP control vector (pSEAP2-Control) was purchased from Clontech, BD Sciences. *p*-Aminophenylphosphate monosodium salt (PAPP) was purchased from LKT Lab Inc. or donated by Prof. Uichi Akiba from Akita University.

2.2. Cell culture and transfection [11,14]

HeLa cells were donated by the Cell Resource Center for Biomedical Research (Tohoku University). The HeLa cells were seeded in a 35 mm dish (Falcon) at a density of 5×10^5 cells in 2 mL of antibiotic-free RPMI-1640 medium containing 10% FBS. On the subsequent day, the cells were transfected with 500 μL of Opti-MEM I medium containing 4 μg of plasmid DNA (pSEAP2-Control, Clontech, BD Sciences) and 10 μL of Lipofectamine™ 2000 and incubated for a further 5 h. Subsequently, the transfection medium was replaced by a fresh culture medium and the cells were incubated overnight at 37 °C.

2.3. Fabrication of single-cell array

The PDMS microwell array was fabricated by using a SU-8 master on a silicon wafer. The SU-8 master was first treated with a silane coupling agent (LS-912) to prevent PDMS from adhering to the master. Next, the PDMS prepolymer was poured on the SU-8 master and cured in the oven at 80 °C for 2 h. After curing, the PDMS replica was peeled off from the SU-8 master and treated with O_2 plasma asher.

2.4. SECM system

The single-cells in the microwell array were further studied by scanning electrochemical microscopy (SECM) [16–20]. The medium containing the cultured cells was poured over the PDMS microwell array. After the cells were trapped in the microwells, the surface was rinsed with a fresh medium to remove the additional cells. Next, the single-cell array was placed in 3 mL of a measuring solution containing 1.0 mM PAPP and HEPES buffer (pH 9.5). A two-electrode system comprising a Pt microdisk (diameter, 20 μm) as the working electrode and an Ag/AgCl reference/counter electrode was employed for the SECM measurements. The position of the Pt microelectrode was controlled with motor-driven *XYZ*-positioner (Chuo-Seiki M9103). Accumulation time (t_{accu}) was defined as the time period accumulating the PAP produced via SEAP reaction within the PDMS microwell. Chronoamperometric (CA) measurements for individual HeLa cells were performed as following steps: Initially the microelectrode was vertically approached the top surface of the PDMS microwell to isolate the volume of the measuring solution surrounded with the walls of the microelectrode and the PDMS microwell. Next, the tip potential was maintained at 0.0 V for t_{accu}. Then, the tip potential was stepped to 0.3 V to oxidize PAP accumulated in the microwell. The vertical position $Z = 0$ was defined at the upper surface of the PDMS microwell.

2.5. Live/dead fluorescence assay on single-cell arrays [11,21]

The viability of the cells patterned on the stencil, under the conditions maintained during SECM measurements, was evaluated using a live/dead fluorescence kit (calcein-AM and PI; Dojindo Laboratories, Japan). The results indicated that almost all the cells were alive for a period of 60 min after being soaked in the measuring solution (pH 9.5).

3. Results and discussion

In this study we have fabricated two types of the PDMS microwell. The one is PDMS microwell without groove. The diameter and the depth of the cylindrical PDMS microwell were designed at 30 μm. The volume of the microwell can be estimated as 21.2 pL. The PDMS microwell array was scanned with 3D Laser scanning microscope (Shimadzu SFT-3500, Japan), the volume was 24.3 ± 1.1 pL ($n = 12$). The other type is PDMS microwell with groove. The width and depth of the groove were both 5 μm. Fig. 1 shows PDMS microwell arrays without and with grooves. Voltammetry at scan rate of 20 mV/s has been performed in a solution containing 4.0 mM ferrocyanide (see Supplemental Data Fig. S1). Voltammograms with limited diffusion behaviors were obtained suggesting that the electric charge of the of the time integration of the oxidation current was reproducibly 7.05 nC when the tip located the top of the PDMS microwell to isolate the volume of the measuring solution. The electric charge value was in good agreement with the theoretical charge estimated from the volume of the solution of 24 pL in the surrounded space with the working electrode and the wall of the PDMS well. Comparing to the previous study, the diameter of the PDMS microwell has been designed a smaller size and the center of the Pt-disk should be aligned carefully. As a same manner, the tip located the top of the PDMS microwell with 5 μm-width groove and voltammetry has been performed. The electric charge value for the PDMS microwell with the groove was 12.5 nC, which was 1.77-fold of that for the PDMS microwell without groove. This result suggested that the volume of the redox species contributing to the oxidation current at the working electrode was 1.77 times larger than that for the PDMS microwell without groove. When the microelectrode located far from the PDMS microwell, a steady state current was obtained and the electric charge value was 3.8×10^2 nC, which was 54-fold of that for the PDMS microwell without groove. These results suggest that the PDMS microwell with groove allows an intermediate situation between the microelectrode located far from the microwell and the microelectrode covering the top of the microwell without groove, from the view point of the reactant mass.

Next we created single-cell array within the PDMS microwell. The HeLa-SEAP individual cells were localized passively within the PDMS microwells. First a suspension of 100 μL culture medium (RPMI 1640) containing 1.0×10^5 cells was put on the PDMS microwell array and stabilized for 5 min. The HeLa-SEAP cell was localized at the bottom of the PDMS microwell with the diameter of 30 μm. The excess cells on the PDMS microwell array were easily removed by manual pipetting. Then the culture medium was

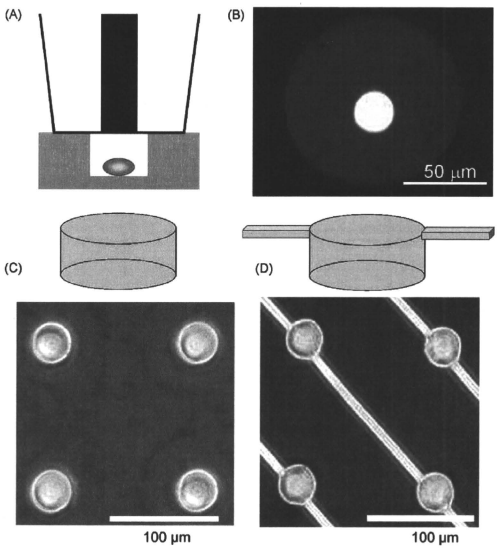

Fig. 1. PDMS microwells without and with grooves. (A) Tip microelectrode was located top of the PDMS microwell to isolate the measuring solution containing single-cell. (B) Microscopic photograph of the tip microelectrode. Pt-disk with 20 μm diameter and glass insulator were seen. (C) PDMS microwell array without groove. (D) PDMS microwell array with groove.

exchanged to the measuring solution containing 1.0 mM PAPP and HEPES buffer (pH 9.5). Because of inappropriate pH of the measuring solution for physiological functions of the cell, it is required to evaluate the cellular viability in the measuring solution.

Fig. 2 shows fluorescence live/dead images for single-cell in PDMS well array after incubation in a pH 9.5 measuring solution for 20 min. It was found that more than 95% cells were alive in the experimental condition. Fig. 2(B) shows a time course of viability (number of cells stained with red fluorescence (dead cell) normalized to all cells in the microwells). In the case of HeLa cells seeded in single-cell array with the PDMS microwell, almost all cells were alive (94%) for a period of 60 min after being soaked in the measuring solution (pH 9.5). It was also found that only 40% were alive for 120 min after incubation. Cellular viability in alkaline solutions strongly depended on the cell types and culture conditions. For example, more than 90% were alive for the cells patterned on a culture dish using a PDMS stencil of 300 μm diameter [10], or with the 180 min incubation in the measuring solution (pH 9.5) at room temperature for A431 cells [21].

Fig. 3 shows CAs for single HeLa-SEAP entrapped in the PDMS microwell without groove. Tip potential was stepped from 0 V to 0.3 V after the tip electrode located top of the PDMS microwell for t_{accu}. Measurement was performed in solution containing 1.0 mM PAPP, HEPES buffer (pH 9.5). Oxidation current increased as t_{accu} became larger; suggesting that the PAP produced via alkaline phosphatase catalysis was accumulated in the PDMS microwell. For wild-type HeLa as shown in Fig. 3(B), the oxidation current response was smaller than that for HeLa-SEAP and the accumulation of PAP in the PDMS microwell was not clear. Even without cell, the current did not reach at zero value and this was probably due to a kind of residual current at +0.3 V in the solution containing PAPP. It is noteworthy here that the SECM response obtained at fixed potential for the PDMS microwell without cell was completely zero [11].

Fig. 4 shows CAs for single HeLa-SEAP entrapped in the PDMS microwell with grooves of 5 μm-width and 5 μm-depth. For the PDMS microwell with groove, the oxidation current response was found to be much larger than that for the PDMS microwell without groove. This is because the enzymatic substrate PAPP was sufficiently supplied to enhance the SEAP catalytic reaction. The produced PAP also efficiently diffused out from the PDMS microwell so that the SEAP catalytic reaction rate was promoted with the groove attached to the PDMS microwell. The oxidation current reached to 70 pA at 50 s after applying the potential step. The current response was large but did not tend to increase with increasing t_{accu}. This result suggested that accumulation within the microwell could not be expected due to the groove. From the view point of sensing system, a larger response can be expected for the PDMS microwell with grooves. However, this kind of time course response might include backgrounds such as capacitance and residual currents and the control experiments for subtracting the background components must be required.

Fig. 5 shows the averaged electric charge (Q, time integration of faraday current from $t = 0$ to 50 s after potential step) estimated from CA. In the case of $t_{accu} = 1$, 11, and 21 min for HeLa-SEAP (filled bars) and wild-type HeLa (open bars). Single-cells were entrapped in microwells without groove (A) and with 5 μm-width groove (B). In Fig. 5(A), the Q value for HeLa-SEAP ($Q_{\text{HeLa-SEAP}}^{\text{without groove}}$) eventually

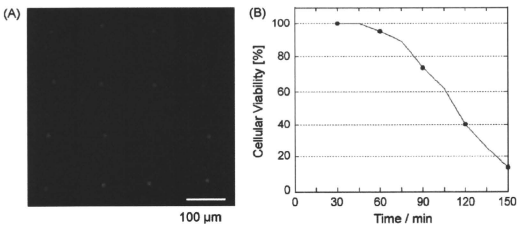

Fig. 2. (A) Fluorescence live/dead images for single-cell in PDMS well array without groove after incubation in a pH 9.5 measuring solution for 20 min. (B) Time course of viability of HeLa cell within the PDMS microwell at pH 9.5.

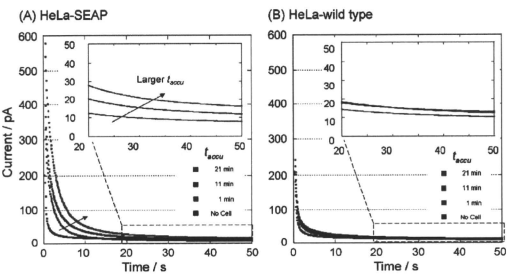

Fig. 3. CAs for single HeLa-SEAP (A) and wild-type HeLa (B) entrapped in the PDMS microwell without groove.

increased as t_{accu} increased. For wild-type HeLa, however, the Q value increase depending on t_{accu} was not evident. In Fig. 5(B), initial $Q_{HeLa\text{-}SEAP}^{with\ groove}$ for t_{accu} = 1 min was much larger than $Q_{HeLa\text{-}SEAP}^{without\ groove}$ in Fig. 5(A), which was reasonable because the oxidation current for the PDMS microwell with groove was larger than that for without groove as shown in Figs. 3 and 4. For both PDMS microwells with and without groove, the response of single wild-type HeLa cell was clearly smaller than HeLa-SEAP. In Fig. 5, the responses for the vacant PDMS microwells with and without groove were also shown. These results were very important to understand the difference of the baseline for each experimental condition including residual current, solution resistance and/or charge current due to electric double layer of the experimental system. Actually, we found the Q for the vacant PDMS microwell with groove ($Q_{no\ cell}^{with\ groove}$) was much larger than that without grove ($Q_{no\ cell}^{without\ groove}$). This suggested that residual current mainly contributed to the $Q_{no\ cell}$ value rather than the double layer electric charge. We can define S/N ratio by subtracting $Q_{no\ cell}$. Namely, the definition of S/N ratio should be $[Q_{HeLa\text{-}SEAP} - Q_{no\ cell}]/[Q_{wild\text{-}type\ HeLa} - Q_{no\ cell}]$ rather than $[Q_{HeLa\text{-}SEAP}/Q_{wild\text{-}type\ HeLa}]$. By considering the discussion above, S/N

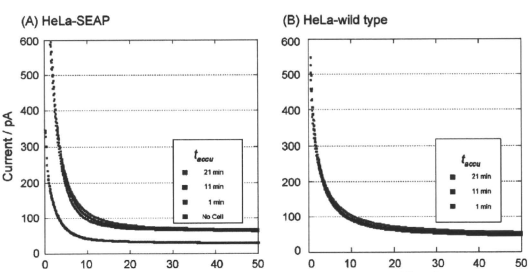

Fig. 4. CAs for single HeLa-SEAP (A) and wild-type HeLa (B) entrapped in the PDMS microwell with grooves of 5 μm-width and 5 μm-depth.

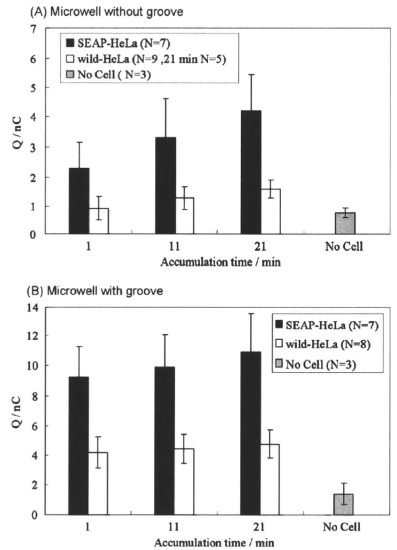

Fig. 5. Shows the averaged electric charge (Q). N indicates the number of the experiment performed for each condition. HeLa-SEAP (filled bars) or wild-type HeLa (open bars) was isolated in the PDMS microwell without (A) and with groove (B). Results for vacant PDMS microwell were also shown (gray bars).

for microwells without groove (S/N = 4.08 at t_{accu} = 21 min) was larger than that with groove (2.80 at t_{accu} = 21 min), nevertheless the $Q_{HeLa\text{-}SEAP}^{without\ groove}$ was smaller than $Q_{HeLa\text{-}SEAP}^{with\ groove}$. It was also found that larger t_{accu} was not effective to obtain larger S/N. For instance, $(S/N)^{without\ groove}$ at = 1, 11, and 21 min, were 9.52, 4.71, and 4.08 respectively. Previously, single-cell SECM imaging was performed for HeLa-SEAP and wild-type HeLa and found that the responses were fluctuated and the averaged responses for HeLa-SEAP normalized to wild-type HeLa was ca. 2.1 [11]. Consequently, the S/N value obtained in the present study was improved by combining CA technique and electric charge analysis.

4. Conclusions

HeLa-SEAP single-cell was localized in PDMS cylindrical microwell arrays with and without groove. Microelectrode was used to cover the top of the PDMS microwell. The product of enzyme reaction within the confined space was accumulated during the t_{accu} and then CA was performed. Almost all HeLa cells were alive for a period of 60 min after being soaked in the measuring solution (pH 9.5). For the PDMS microwell without groove, the electric charge value increased as increasing t_{accu}, suggesting that the PAP produced via SEAP catalysis was effectively accumulated in the PDMS microwell. On the contrary, for the PDMS microwell with groove, the current response was large but did not tend to increase with increasing t_{accu}. The shape of the depressed well allows a larger current value and rapid response compared to the confined well design and preferential for high-throughput single-cell screening.

Acknowledgement

This work was partly supported by Grants-in-Aid for Scientific Research (18101006, 21685008 and 21106502) from MEXT; and by a grant from the Center for Interdisciplinary Research, Tohoku University.

Appendix A. Supplementary data

Supplementary data associated with this article can be found, in the online version, at doi:10.1016/j.electacta.2010.04.011.

References

[1] A. Raj, A. van Oudenaarden, Cell 135 (2008) 216.
[2] H.H. Chang, M. Hemberg, M. Barahona, D.E. Ingber, S. Huang, Nature 453 (2008) 544.
[3] J. Hanna, K. Saha, B. Pando, et al., Nature 462 (2009) 595.
[4] M. Bengtsson, A. Ståhlberg, P. Rorsman, M. Kubista, Genome Res. 15 (2005) 1388.
[5] J.F. Zhong, Y. Chen, J.S. Marcus, A. Scherer, S.R. Quake, C.R. Taylor, L.P. Weiner, Lab Chip 8 (2008) 68.
[6] K. Taniguchi, T. Kajiyama, H. Kambara, Nat. Methods 6 (2009) 503.
[7] Y. Nashimoto, Y. Takahashi, T. Yamakawa, Y.S. Torisawa, T. Yasukawa, T. Ito-Sasaki, M. Yokoo, H. Abe, H. Shiku, H. Kambara, T. Matsue, Anal. Chem. 79 (2007) 6823.
[8] M. Badihi-Mossberg, V. Buchner, J. Rishpon, Electroanalysis 19 (2007) 2015.
[9] E. Kelso, J. McLean, M.F. Cardosi, Electroanalysis 12 (2000) 490.
[10] H. Shiku, M. Takeda, T. Murata, U. Akiba, F. Mizutani, T. Matsue, Anal. Chim. Acta 640 (2009) 87.
[11] T. Murata, T. Yasukawa, H. Shiku, T. Matsue, Biosens. Bioelectron. 25 (2009) 913.
[12] Z. Lin, Y. Takahashi, T. Murata, M. Takeda, K. Ino, H. Shiku, T. Matsue, Angew. Chem. Int. Ed. 48 (2009) 2044.
[13] Y. Takahashi, H. Shiku, T. Murata, T. Yasukawa, T. Matsue, Anal. Chem. 81 (2009) 9674.
[14] Y.S. Torisawa, N. Ohara, K. Nagamine, S. Kasai, T. Yasukawa, H. Shiku, T. Matsue, Anal. Chem. 78 (2006) 7625.
[15] K.Y. Inoue, T. Yasukawa, H. Shiku, T. Matsue, Electrochemistry 76 (2008) 525.
[16] H. Shiku, S. Goto, S. Jung, K. Nagamine, M. Koide, T. Itayama, T. Yasukawa, T. Matsue, Analyst 134 (2009) 182.
[17] G. Wittstock, M. Burchardt, S.E. Pust, Y. Shen, C. Zhao, Angew. Chem. Int. Ed. 46 (2007) 1584.
[18] A. Schulte, W. Schuhmann, Angew. Chem. Int. Ed. 46 (2007) 8760.
[19] X. Li, A.J. Bard, J. Electroanal. Chem. 628 (2009) 35.
[20] L. Diaz-Ballote, M. Alpuche-Aviles, D.O. Wipf, J. Electroanal. Chem. 604 (2007) 17.
[21] Y. Takahashi, T. Miyamoto, H. Shiku, R. Asano, T. Yasukawa, I. Kumagai, T. Matsue, Anal. Chem. 81 (2009) 2785.

Electrochemical topography of a cell monolayer with an addressable microelectrode array†

Zhenyu Lin,[ab] Kosuke Ino,[a] Hitoshi Shiku[a] and Tomokazu Matsue[a]

Received (in Cambridge, UK) 27th July 2009, Accepted 17th November 2009
First published as an Advance Article on the web 4th December 2009
DOI: 10.1039/b915212a

The present study describes a new electrochemical imaging method for monitoring the population and growth of adherent cells with a novel addressable microelectrode array.

Cell-based assays refer to any experiment that is based on the use of live cells. These include a variety of methods for measuring cell viability, cytotoxicity, proliferation, motility, and morphology.[1] Advanced imaging methods for living cells can help to clarify the mechanisms of metabolism as well as the influence of environmental pollutants on animal and plant cells.[2] More than 70% of malignant tumors are of epithelial origin[3] and, therefore, studying cell adhesion is a pertinent topic. Microscopic observation and characterization of living cells have mostly been performed with optical microscopes, since shape, topography, and even cellular functions controlled by cell binding to the scaffolds can be easily evaluated by optical instruments. However, non-optical techniques can also uncover the status of cell adhesion and can easily determine whether cells are adherent. For instance, impedance spectroscopy with microelectrode arrays has been implemented to monitor cell attachment, internalization of functional materials, and differentiation.[4–7] When cells attach to an electrode substrate, the adherent cells passively block the current flow and the impedance of the electrode increases. Therefore, impedance measurements have been applied to detect cellular density, growth, and alterations under the physiological state of the cells during cultivation in real-time.[8–11] This technique has also been established to monitor cellular behavior at the microelectrode surface.[12,13] Other methods, such as a scanning electrochemical microscope or a QCM-D (quartz crystal microbalance with dissipation) have also been applied to cell studies.[14,15] But until now, little attention has been paid to amperometric detection schemes for the study of cell topography.

We recently communicated the basic principle of a novel multipoint addressable electrochemical device that consisted of an orthogonally arranged row/column array of electrodes.[16,17] A high-throughput screen system was established on the basis of redox cycling at the crossing points of the row/column electrodes. With this system, the electrochemical response at

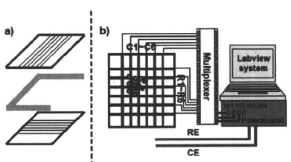

Fig. 1 (a) The layered structure of the device. From top to bottom: column electrodes (width: 50 μm), Su-8 sheet and row electrodes (width: 50 μm); the middle and bottom layer adhered to each other. (b) The scheme of the detection system. The points on the microchip indicate the cells.

100 individual addressing points could be measured in 22 s. The device can also be used for electrochemical imaging on the basis of the blocking effect of redox cycling by the cell adhesion. Since cell adhesion blocks redox cycling at the addressable point of the device to reduce current responses, it is possible to perform electrochemical imaging of cell topography. In this study, an amperometric imaging technique was developed using the above principle and was applied to the monitoring of cell proliferation. With this technique, cell distribution, growth, and death were successfully imaged with an addressable device consisting of orthogonally located array electrodes.

A microelectrode chip with a 6 column electrode and a 6 row electrode was fabricated and applied for cell image detection. Fig. 1 shows the scheme of the detection system (the detail fabrication procedure is shown in ESI†).

It is possible to qualitatively and quantitatively study the electrochemical performance of the microelectrode array by cyclic voltammetry. Fig. 2 shows cyclic voltammograms of 4.0 mM $K_3[Fe(CN)_6]$ in 0.1 M KCl at the same column electrodes (C2) under different conditions. For curve a, only C2 was swept with potential while the other column electrodes

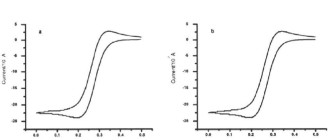

Fig. 2 Cyclic voltammograms for a column microband electrode (C2) in 4 mM $K_3[Fe(CN)_6]$ and 0.1 M KCl. Voltage was applied to (a) an individual column microelectrode (C2) or (b) all 6 column microelectrodes simultaneously but only C2 was read out. Scan rate: 50 mV s^{-1}.

[a] *Graduate School of Environmental Studies, Tohoku University, 6-6-11 Aoba, Aramaki, Sendai 980-8579, Japan. E-mail: matsue@bioinfo.che.tohoku.ac.jp; Fax: +81-22-795-7209*
[b] *Ministry of Education Key Laboratory of Analysis and Detection Technology for Food Safety, Department of Chemistry, Fuzhou University Fuzhou, Fujian 350002, China. Fax: (+86)591-83713866*
† Electronic supplementary information (ESI) available: Fabrication of microelectrode array, instrumentation, cell pattern preparation and detection procedure. See DOI: 10.1039/b915212a

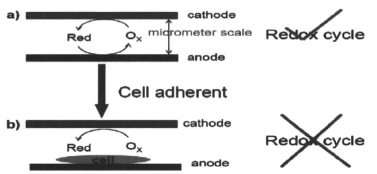

Fig. 3 The principle for cell topography detection. (a) Before cell adhesion; (b) after cell adhesion.

were kept open. For curve b, all column electrodes (C1–C6) had the same potential applied simultaneously, but only the current at C2 was read out. Both curves show a sigmoidal shape. In addition, the two curves show nearly identical behavior. This feature implies that the individual diffusion layers from the adjacent column electrodes did not overlap and, therefore, there was no interference from cross-talk between the column electrodes during the detection period.

The principle of cell topography imaging is shown in Fig. 3. If the redox compound showing reversible electrochemical behavior is present in the interspaces between the column and row electrodes set at appropriate potentials, the reduction and oxidation of the compound proceeds at the addressing point. This redox cycling, proceeding only at the designated addressing point, amplifies the electrochemical signal[16,17] (Fig. 3(a)). Since the magnitude of the amplified current has a direct relationship with the area of the electrode,[18] the current response or amplification efficiency becomes lower when the electrode at the addressing points is covered with insulating material, such as living cells. Therefore, the redox cycling will be blocked and the current amplification will be reduced (Fig. 3(b)) if cells grow adherently on the electrode surface at an addressing point. By sequentially changing the potential applied to different column and row electrodes and the read-out column electrode, as described in the experimental section, the current responses at each addressing point can be obtained to draw two-dimensional electrochemical responses, which in turn indicates the topography of the cells.

In our earlier study, a 4-aminophenol (PAP) and *p*-quinoneimine redox cycling system was used to study gene expression ability in single cells,[17] since PAP is a cellular membrane-permeable substance. To obtain a clear image based on the blockage of redox cycling, it is desirable to use a non-permeable redox species; thus, $K_3[Fe(CN)_6]$ was chosen as the species in this study, since $Fe(CN)_6^{3-}$ is non-permeable through the cell membrane.

In order to monitor cell topography and proliferation, it is necessary that the cells remain viable after detection. Cell viability was checked using Calcein-AM (Wako Pure Chemical Industries, Tokyo, Japan) and it was confirmed that all of the cells were alive for at least 30 min in the detection medium. Since the electrochemical detection in the medium was completed within 10 min, there should have been no significant influence on the viability during the electrochemical detection.

Before cell adhesion, the current amplification at each addressing point was investigated. The RSD (relative

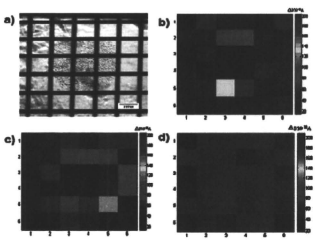

Fig. 4 (a) The image of cell topography obtained by microscopy, (b) the corresponding current image, (c) the current image after 24 h of additional cultivation, and (d) after treating with 2% methanol.

standard deviation) of the current amplification at the addressing points was 2.87%, indicating that all of the addressing points were under electrochemically equivalent circumstances. When the cell suspension in the detection medium with 4.0 mM $Fe(CN)_6^{3-}$ was introduced into the chip, the current responses or amplification efficiencies were found to be similar to those without the cells. This result indicates that the floating cells did not block the redox cycling of the $Fe(CN)_6^{3-}/Fe(CN)_6^{4-}$ redox couple at the addressing points.

Next, the electrochemical imaging of the cells on the substrate was investigated using the addressable device. Fig. 4 shows the optical photograph of the patterned cells and the electrochemical images observed with the addressable device. The area with low electrochemical responses (Fig. 4(b)) corresponds well with that of the topography of the patterned cells in the optical photograph (Fig. 4(a)), since the cells blocked the redox cycling of $Fe(CN)_6^{3-}/Fe(CN)_6^{4-}$. After the measurement, the device was disassembled and the cells were cultured for 24 h. The electrochemical image after the cultivation shows that the topography with low currents expanded (Fig. 4(c)) compared to the image in Fig. 4(b). During the cultivation, the HeLa cells proliferated and expanded the topography of the cell pattern on the substrate, causing partial coverage of the surrounding crossing points. This coverage decreased the amplification efficiency by redox cycling and lowered the current responses at the crossing points. With further cell culture, the area with low current responses became larger.

An *in vitro* cytotoxicity assay was considered as a promising alternative method to animal testing and has been applied to determine basic cytotoxicity and cell viability assessment. In the assay, the key issue was how to assess the numbers of viable and non-viable cells after exposure to special chemicals.[19] In the present study, we applied the proposed addressable device for cytotoxicity detection. Methanol was chosen as a toxic chemical for the model case. It is known that a solution containing 2% methanol is fatal to cells. After a clear topography of the patterned cells was observed (Fig. 4(c)), the solution inside the addressable device was changed to 4.0 mM $K_3[Fe(CN)_6]$ containing 2% methanol. The electrochemical responses at the topography area

increased gradually and reached a constant in 5 min. After 5 min, no topography was found in the electrochemical image (Fig. 4(d)). The methanol in the solution caused fatal damage to the cells, which detached from the substrate, thus leading to a recovery in redox cycling and current amplification at the crossing points. Thus, the topography of the cell pattern faded out from the electrochemical image on exposure to 2% methanol. These results indicate that the present electrochemical device is applicable for the investigation of cytotoxicity of various species.

The present study demonstrated an electrochemical method for detecting cell topography using an addressable electrochemical device with orthogonally arranged row/column electrode arrays. The presence of adherent cells at the addressing points blocks redox cycling between the row and column electrodes because the redox species do not permeate through the cell membrane. This blockage reduces the current response based on redox amplification. Since the current response depends on the status of the cells, concentration, proliferation of the adherent cells, and cytotoxicity effects can be monitored or imaged with the device. The present device can be applied to cell culture toxicology tests. Although in the present device, there is a problem with the changing of the solution, integration with a solution-changing system could facilitate the replacement of the solution in the gap regions between the row and column electrodes to make the device easier to handle when applying it to cytotoxicity studies. Further work in this direction is underway at our laboratory.

This study was supported by Special Coordination Funds for Promoting Science and Technology, Formation of Innovation Center for Fusion of Advanced Technologies, from Japan Science and Technology Agency, and by a Grant-in-Aid (445) for Science Research on Priority Areas "Life Surveyor" from MEXT, Japan. Z.Y also thanks the support of the National Basic Research Program of China (No. 2010CB732403), the NSFC (20735002,20905013), and the Special Foundation for Young Scientists of Fujian Province, China (2008F3057).

Notes and references

1 J. H. Yeon and J.-K. Park, *Anal. Biochem.*, 2005, **341**, 308.
2 R. E. White, *Annu. Rev. Pharmacol. Toxicol.*, 2000, **40**, 133.
3 B. Henderson, R. K. Ross and M. C. Pike, *Science*, 1991, **254**, 1131.
4 I. Giaever and C. R. Keese, *Proc. Natl. Acad. Sci. U. S. A.*, 1984, **81**, 3761.
5 I. Giaever and C. R. Keese, *Nature*, 1993, **366**, 591.
6 Y. L. Qiu, R. L. Liao and X. Zhang, *Anal. Chem.*, 2008, **80**, 990.
7 A. Chatterjee, C. Snead, G. Yetik-Anacak, G. Antonova, J. M. Zeng and J. D. Catravas, *Am. J. Physiol.: Lung Cell. Mol. Phys.*, 2008, **294**, L755.
8 C. Xiao and J. H. T. Luong, *Biotechnol. Prog.*, 2003, **19**, 1000.
9 L. Ceriotti, J. Ponti, F. Broggi, A. Kob, S. Drechsler, E. Thedinga, P. Colpo, E. Sabbioni, R. Ehret and F. Rossi, *Sens. Actuators, B*, 2007, **123**, 769.
10 N. C. Yu, J. M. Atienza, J. Bernard, S. Blanc, J. Zhu, X. B. Wang, X. Xu and Y. A. Abassi, *Anal. Chem.*, 2006, **78**, 35.
11 K. T. C. Chai, J. H. Daview and D. R. S. Cumming, *Sens. Actuators, B*, 2007, **127**, 97.
12 E. E. Krommenhoek, J. G. E. Gardeniers and J. G. Bomer, *Anal. Chem.*, 2007, **79**, 5567.
13 R. Ehret, W. Baumann, M. Brischwein, A. Schwinde, K. Stegbauer and B. Wolf, *Biosens. Bioelectron.*, 1997, **12**, 29.
14 L. Pitta Bauermann, W. Schuhmann and A. Schulte, *Phys. Chem. Chem. Phys.*, 2004, **6**, 4003.
15 C. Modin, L. Stranne, M. Foss, M. Duch, J. Justesen, J. Chevallier, L. K. Andersen, A. G. Hemmersam, F. S. Pedersen and F. Besenbacher, *Biomaterials*, 2006, **27**, 1346.
16 Z. Y. Lin, Y. Takahashi, Y. Kitagawa, T. Umemura, H. Shiku and T. Matsue, *Anal. Chem.*, 2008, **80**, 6830.
17 Z. Y. Lin, Y. Takahashi; T. Murata, M. Takeda, K. Ino, H. Shiku and T. Matsue, *Angew. Chem., Int. Ed.*, 2009, **48**, 2044.
18 T. Matsue, A. Aoki, T. Abe and I. Uchida, *Chem. Lett.*, 1989, 133.
19 F. Zucco, I. De Angelis, E. Testai and A. Stammati, *Toxicol. in Vitro*, 2004, **18**, 153.

Addressable electrochemiluminescence detection system based on redox-cycling of $Ru(bpy)_3^{2+}$†

Zhenyu Lin,[a] Kosuke Ino,[b] Hitoshi Shiku,[b] Tomokazu Matsue*[b] and Guonan Chen*[a]

Received (in Cambridge, UK) 4th August 2009, Accepted 22nd October 2009
First published as an Advance Article on the web 16th November 2009
DOI: 10.1039/b915871e

This is the first report on addressable electrochemiluminescence (ECL) based on redox-cycling of tris(2,2′-bipyridine)-ruthenium(II) ($Ru(bpy)_3^{2+}$). By changing the column or row electrodes addressed, the ECL at each address point can be detected separately.

Electrochemiluminescence (ECL) is a chemiluminescent reaction of species generated electrochemically at an electrode surface, which is a sensitive and selective detection method having important applications in bioanalytical science. The ECL of tris(2,2′-bipyridine)-ruthenium(II) ($Ru(bpy)_3^{2+}$) was one of the mostly studied ECL systems since its first publication in 1966.[1-4] Different mechanisms can lead to the ECL of $Ru(bpy)_3^{2+}$, such as coreactant and annihilation ECL systems.[5] In the latter system, $Ru(bpy)_3^{2+}$ can be oxidized and reduced on a single electrode with high frequency to produce $Ru(bpy)_3^{3+}$ and $Ru(bpy)_3^{+}$, respectively, then the annihilation reaction between these two productions occurs to produce the excited $[Ru(bpy)_3^{2+}]^*$ and further to give ECL.[6] $Ru(bpy)_3^{2+}$ showed the character of redox-cycling during ECL reactions, the amount of $Ru(bpy)_3^{2+}$ had not been reduced. It is also possible to obtain emission at two different electrodes that are close enough to allow the electrogenerated reactants to interdiffuse and undergo annihilation.[7] For example, a rotating ring disk electrode can be applied to generate one reactant at the central disk while the other one is generated at the ring, then these two reactants diffuse and react to produce ECL.[8] Murry *et al.* studied the ECL of $Ru(bpy)_3^{2+}$ on micrometer-spaced platinum interdigitated electrodes.[9] Annihilation ECL with microelectrodes has been used to study sol–gel composites containing $Ru(bpy)_3^{2+}$ and diode-like chemiluminescence in frozen concentration gradients of the polymer poly-$[Ru(vbpy)_3](PF_6)_2$.[10] Hayase *et al.* used transparent conductive glass as two working electrodes, which were arranged face to face, with a gap left between the electrodes, it showed that high ECL intensity could be detected if the $Ru(bpy)_3(PF_6)_2$ being injected into the gap and the two electrodes had been set at an appropriate potential.[11] Michel *et al.* reported that protein–ruthenium chelate complexes could lead to redox-cycling type ECL in aqueous medium.[12] Based on this result, it is possible to develop the immunoassays involving redox-cycling type ECL as the detection principle. These studies showed it is easy to control the ECL by dual-working electrode systems and can lead to real applications.

In order to realize rapid, comprehensive and high-throughput analyses, there has been strong demand to develop array-based biosensors. Many array-based biosensors developed so far are based on fluorescence detection since fluorescence measurement usually has a high sensitivity. Another form of detection utilized in array-based biosensors is amperometric detection, which offers sufficient sensitivity as well as specificity. ECL detection has also been applied in array-based sensors. For example, Sojic *et al.* had developed an ordered array of optoelectrochemical, individually readable sensors which had an application in remote ECL imaging.[13] The sensors of the array can not be individually addressable electrochemically detected, but each addressable point is optically independent and individually readable.

In an early study, we put forward a novel electrochemical image system, which consisted of orthogonally arranged row/column electrode arrays, which have the benefits of easy fabrication and high integration.[14,15] Based on the redox-cycling of some electroactive compounds at the crossing points of the row/column electrodes, electrochemical response at each addressing point can be detected separately. In this research, detection of the $Ru(bpy)_3^{2+}$ ECL system has been coupled to the proposed device and a simple ECL image system has been developed. The two microelectrodes at the crossing points can be deemed as the dual-working electrode in the annihilation ECL reaction of $Ru(bpy)_3^{2+}$. Changing the addressing of the column and row electrodes, the crossing point will be changed too. In this way, the ECL at each crossing point can be detected separately or simultaneously.

Fig. 1(A,B) shows the scheme of the addressable micro-electrode array. Two platinum microbands (width: 50 μm; gab between the two microbands: 250 μm) were constructed on a glass substrate by using a photolithographic method.[14,15] Two holes were then made on one substrate by a CO_2 laser (M class, Universal Laser Systems, AZ, USA), the holes will serve as the inlet and the outlet for the ECL solution. The Su-8 sheet (15-μm thick; Nippon Kayaku Co. Ltd. Japan) was cut to required specifications and then two glass substrates with the microelectrode array were orthogonally glued face to face through the Su-8 sheet using a hard-bake (180 °C), and formed 4 orthogonal crossing points. The gap between the two substrates can contain solutions and act as a reaction well. The scheme of the ECL detection system was shown in Fig. 1(C), the detail of which is shown in the ESI.†

Fig. 2 highlights the principle of the row/column array architecture addressable ECL detection. During testing, the

[a] *The Key Lab of Analysis and Detection Technology for Food Safety of the MOE, Department of Chemistry, Fuzhou University, Fuzhou, 350002, China. E-mail: gnchen@fzu.edu.cn*
[b] *Graduate School of Environmental Studies, Tohoku University, 6-6-11 Aoba, Aramaki, Sendai 980-8579, Japan. E-mail: matsue@bioinfo.che.tohoku.ac.jp; Fax: (+86)591-83713866*

† Electronic supplementary information (ESI) available: Experimental details. See DOI: 10.1039/b915871e

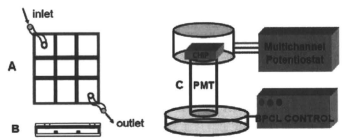

Fig. 1 Scheme of the addressable chip and the ECL detection chip. (A): top view of the chip; (B): side view of the chip; (C): scheme of the ECL detection system.

column and the row electrodes at the addressing points have been applied with appropriate potentials, one with oxidation potential and the other at the reduction potential, while all the other working electrodes were left open. When oxidation potential was applied to the addressed column electrode, $Ru(bpy)_3^{2+}$ could be oxidized to $Ru(bpy)_3^{3+}$, while $Ru(bpy)_3^{+}$ would be produced at the addressed row electrode, where a reduction potential had been applied. Then $Ru(bpy)_3^{3+}$ and $Ru(bpy)_3^{+}$ would diffuse from the electrode to the main solutions to react to produce the excited $[Ru(bpy)_3^{2+}]^*$. When $[Ru(bpy)_3^{2+}]^*$ goes back to its basic state, it produces ECL signals. From this mechanism, we know that in one reaction circle, the luminescent reagent has not been consumed, which shows the character of redox-cycling.

Of the other points on the chosen column or row electrodes, only $Ru(bpy)_3^{3+}$ or $Ru(bpy)_3^{+}$ has been produced, which cannot generate an ECL signal. While on the other electrodes that have not been addressed, no reaction happened. In this case, the ECL signals just come from the addressed points. By sequentially changing the potential applied to the column and row electrodes, we collected the ECL responses at the entire crossing point, allowing the system to be addressable. We can address different electrodes at the same time, in this case, we can detect the total ECL intensity from many addressing points.

The cyclic voltammogram of 1 mM $Ru(bpy)_3^{2+}$ had been examined, and it was found that on the anodic side, a clear peak could be observed at 1.2 V *versus* Pt, which was attributed to the redox cycle of $Ru(bpy)_3^{2+}/Ru(bpy)_3^{3+}$. On the cathodic side, another peak corresponding to the redox cycle of $Ru(bpy)_3^{2+}/Ru(bpy)_3^{+}$ appeared at −1.3 V. So in this study, 1.2 and −1.3 V were chosen. Fig. 3 shows the current and ECL recorded on one addressable point. From Fig. 3,

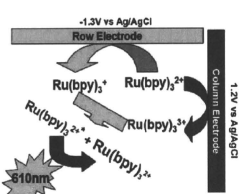

Fig. 2 Principle of the ECL reaction based on redox-cycling.

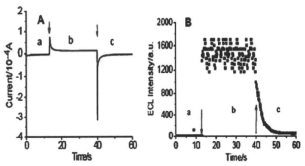

Fig. 3 Current recorded for one column electrode at a single addressing point (A) and the corresponding ECL signal recorded (B). a: Column electrode 1.20 V, row electrode open; b: Column electrode 1.2 V, row electrode −1.3 V; c: Column electrode 1.2 V, row electrode open. $Ru(bpy)_3^{2+}$: 8.0×10^{-8} mol L^{-1}.

it can be seen that only oxidation and reduction potentials have been applied on the crossing electrodes, the ECL signal could be detected. And the detection current can be enhanced also based on redox-cycling.

The relationship between the ECL intensity and the gap has also been studied. The results showed that the ECL intensity decreased significantly with increasing distance. The same results can be found on the current amplification. We also found that if the distance was larger than 150 μm, only a weak ECL signal could be detected, the reasons might be due to the fact that the distance was outside the region of the expected diffusion layer, so $Ru(bpy)_3^{3+}$ and $Ru(bpy)_3^{+}$ had very little chance of meeting together to produce ECL.

By applying the appropriate potential on the micro-electrodes, we sequentially detected the ECL from different addressing points. The results are shown in Fig. 4(A), the ECL intensities at each point showed good reproducibility, the deviation was lower than 5%, which indicated that it was easy to solve the problem of poor reproducibility in ECL detection by this method. We partly covered two addressing points with 5 μm-thick SU-8, since the oxidation of $Ru(bpy)_3^{2+}$ had been blocked, no ECL signals had been detected. If we addressed two points at the same time, the ECL intensity would be double too. These results also indicated that no cross talking happened between the neighbor points. If a transparent material, such as ITO was used as the working electrode, and a sensitive CCD camera was used for detection of ECL signal, the separated points on the chip might be detected simultaneously.

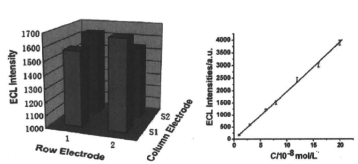

Fig. 4 (A) ECL intensities of 8.0×10^{-8} mol L^{-1} $Ru(bpy)_3^{2+}$ recorded at four different addressing points. (B) The relationship between ECL intensity and $Ru(bpy)_3^{2+}$ concentration.